The encapsulation efficiency of zircon pigments from robust solids to clear solutions

Shan Peng and Ranran Yang
School of Materials Science and Engineering, Hubei University, Wuhan, China
Binglong Lei
School of Materials Science and Engineering, Hubei University, Wuhan, China and Jinhuan Pigments Co., Ltd, Yichun, China
Yun Gao
School of Materials Science and Engineering, Hubei University, Wuhan, China
Renhua Chen
Jinhuan Pigments Co., Ltd., Yichun, China, and
Xiaohong Xia and Kevin P. Homewood
School of Materials Science and Engineering, Hubei University, Wuhan, China

Abstract

Purpose – This paper aims to systematically demonstrate a methodology to determine the relative and absolute encapsulation efficiencies (α_{Re} and α_{Ab}) for thermally- and chemically-robust inorganic pigments, typically like $ZrSiO_4$-based pigments, thereby enhancing their coloring performance.

Design/methodology/approach – The authors designed a route, surplus alkali-decomposition and subsequently strong-acid dissolution (SAD2) to completely decompose three classic zircon pigments (Pr–$ZrSiO_4$, Fe_2O_3@$ZrSiO_4$ and CdS@$ZrSiO_4$) into clear solutions and preferably used inductively coupled plasma-optical emission spectrometry (ICP-OES) to determine the concentrations of host elements and chromophores, thereby deriving the numeric data and interrelation of α_{Re} and α_{Ab}.

Findings – Zircon pigments can be thoroughly decomposed into some dissoluble zirconate–silicate resultants by SAD2 at a ratio of the fluxing agent to pigment over 6. ICP-OES is proved more suitable than some other quantification techniques in deriving the compositional concentrations, thereby the values of α_{Re} and α_{Ab}, and their transformation coefficient K_{RA}, which maintains stably within 0.8–0.9 in Fe_2O_3@$ZrSiO_4$ and CdS@$ZrSiO_4$ and is slightly reduced to 0.67–0.85 in Pr–$ZrSiO_4$.

Practical implications – The SAD2 method and encapsulation efficiencies are well applicable for both zircon pigments and the other pigmental or non-pigmental inhomogeneous systems in characterizing their accurate composition.

Originality/value – The authors herein first proposed strict definitions for the relative and absolute encapsulation efficiencies for inorganic pigments, developed a relatively stringent methodology to determine their accurate values and interrelation.

Keywords Zircon, $ZrSiO_4$, Pigments, Silicates, Encapsulation

Paper type Research paper

1. Introduction

Zircon-based pigments (or encapsulated pigments) possess copious tunable hues, intense tinting strength and excellent compatibility with many other inorganic pigments and are, hence, widely investigated and applied for decoration of ceramics, plastics, paints and coatings (Wang *et al.*, 2022a, 2022b; Yang *et al.*, 2021; Tang *et al.*, 2019; Qin *et al.*, 2021; Jansen and Letschert, 2000). These zircon pigments can serve as a paradigm to explore the correlation of a coloring component in the matrix and the chromatic performance for most of robust inorganic pigments. The concentration of chromophores usually acts dominantly in determining the final pigmental hue through sufficient light absorption–reflection in visible lights. Therefore, it is of great significance to determinate the accurate concentration of the coloring centers in an allochromatic pigmentation system.

According to the distinction of the coloring mechanism, zircon pigments are generally divided into two subcategories: (I) heteromorphic zircon pigments (HMZPs), represented by the brilliant red $CdSe_xS_{1-x}$@$ZrSiO_4$, yellow CdS@$ZrSiO_4$, carbon-black C@$ZrSiO_4$ and iron-red Fe_2O_3@$ZrSiO_4$

The current issue and full text archive of this journal is available on Emerald Insight at: **https://www.emerald.com/insight/0369-9420.htm**

Pigment & Resin Technology
 [ISSN 0369-9420]
[DOI 10.1108/PRT-12-2022-0147]

The authors work is financially supported by the National Natural Science Foundation of China (No. 51602096, 12174092, 11874144, 21801071), China Postdoctoral Science Foundation (2020M682382), Hubei Provincial Department of Science and Technology (2018CFA026, 2019CFA079), Wuhan Science and Technology Bureau (No. 2018010401011268), and the Program of Introducing Talents of Discipline to Universities ("111 Project", D18025). S. Peng and R. Yang contributed equally to this work.

Received 20 December 2022
Revised 10 February 2023
Accepted 11 February 2023

(Qin *et al.*, 2021; Chen *et al.*, 2019; Cannio and Bondioli, 2012); (II) ion-substitutional zircon pigments (ISZPs), typically as the yellow Pr–$ZrSiO_4$, green Cr–$ZrSiO_4$ and the blue V–$ZrSiO_4$ (Yang *et al.*, 2021; Zhang *et al.*, 2021; Guo *et al.*, 2018; Li *et al.*, 2019). Both of the two types belong to allochromatic pigments and, to date, have yet to advance to their vertex stage of development; even the well-established Pr–$ZrSiO_4$ yellow, for instance, still has a much inferior tinting strength to that of $BiVO_4$ and $PbCrO_4$ (as typical idiochromatic pigments), whereas the Cr–$ZrSiO_4$ green and the V–$ZrSiO_4$ blue possess their best chroma C^* only below 40 (in contrast, the $CoAl_2O_4$ blue with C^* exceeding 70) (Yang *et al.*, 2021; Zhang *et al.*, 2021; Li *et al.*, 2019; Zhang *et al.*, 2019). The pivotal impediment originates from the suboptimal encapsulation of the zircon matrix to chromophores, and however, this can be enhanced in future, e.g. by virtue of cation-splitting and optimizing the light reflection–absorption. A foremost task is, therefore, to determine the content of coloring centers in the zircon matrix, namely, the encapsulation efficiency (Lei *et al.*, 2015; Tang *et al.*, 2018; Chen *et al.*, 2018), which is a vital index to evaluate the chromatic quality of the pigments.

To date, there has been no reliable methodology to determine the numeric value of the encapsulation efficiency of zircon pigments, although its concept had been proposed nearly one decade ago (Lei *et al.*, 2015; Chen *et al.*, 2018; Heydari *et al.*, 2013). This is attributed mostly to the extremely high thermo- and chemical-stability of zircon, which can readily withstand temperatures up to 1,200–1,400°C even in a corrosive molten ceramic glaze (Wang *et al.*, 2015; Wang *et al.*, 2020). However, it is a prerequisite to realize complete decomposition of the zircon pigments for accurate compositional quantification. There were studies that had explored the zircon decomposition, typically by virtue of base fusion at 800–1,100°C with alkali metal oxides or hydroxides, e.g. NaOH, K_2SiF_6 or Na_2CO_3 (Abdelkader *et al.*, 2008; Sun *et al.*, 2019). In general, it was not necessary and also inaccessible to completely decompose the zircon materials if the conduction was done only for extraction of zirconia or silica (Sun *et al.*, 2019; Zhang *et al.*, 2012) rather than for determining the real composition of a zircon product.

Simultaneously, a suitable quantitative analysis also arises as another critical concern in determining encapsulation efficiency. The techniques for compositional elements in the material sciences generally include X-ray photoelectron spectroscopy (XPS), energy/wavelength dispersive spectroscopy (EDS/WDS), X-ray fluorescence (XRF), inductively coupled plasma-optical emission spectrometry or mass spectrometry (ICP-OES/MS), atomic absorption spectroscopy (AAS), electron probe microanalysis (EPMA), laser-ablation ICP-MS (LA-ICP-MS) and secondary ion-MS (SIMS), *etc.* Every technique possesses its pros and cons when applied to characterize the zircon pigments, which typically have average sizes ranging 3–20 μm (Tang *et al.*, 2019; Guo *et al.*, 2018; Lei *et al.*, 2015) and, more importantly, have part of their coloring centers (especially in HMZPs) embedded 0.5–5 μm below the zircon shell. For the non-destructive XPS, EDS XRF and EPMA, they in nature belong to semi-quantitative and/or shallow-surficial analyses (signaling depth $<$1.0 μm) and are hence disqualified to determine the accurate composition of the inhomogeneous zircon pigments (especially HMZPs). Although LA-ICP-MS and SIMS have extraordinarily high accuracy, they alike are unsuitable for zircon pigments due to their disadvantages of severe elemental fractionation in atomization and also suitability solely for large crystals (typically over 100 μm) for the stable immobilization to accept steady bombardment from laser or secondary ions projected upon areas generally over 20 μm in diameter (Ver Hoeve *et al.*, 2018; Hou *et al.*, 2020). Therefore, suitable quantification resides primarily to ICP-OES/MS and AAS, which equally belong to destructive techniques and can only produce remarkable accuracy from real solutions or superfine colloids without apparent precipitates. It becomes necessitated to decompose the zircon pigments first for determining the content of coloring centers.

We here presented a route, surplus alkali-decomposition and strong acid dissolution to realize completely decompose three types of zircon-based allochromatic pigments, Pr–$ZrSiO_4$, Fe_2O_3@$ZrSiO_4$ and CdS@$ZrSiO_4$, and thereby determined the concentration of their chromophores by ICP-OES. Accordingly, the relative/absolute encapsulation efficiencies (α_{Re} and α_{Ab}, respectively) were proposed in definition and determined in value; their correlation and the chromatic performance of the pigments were also explored. Our work tackles a tricky challenge confronting the inorganic pigments, which have a zircon or zircon-like robust matrix and can still be advanced for improved performance in application.

2. Materials and methods

2.1 Materials

Analytical-grade zirconium oxychloride ($ZrOCl_2{\cdot}8H_2O$), ferrous sulfate ($FeSO_4{\cdot}7H_2O$), cadmium sulfate ($CdSO_4{\cdot}8/3H_2O$), sodium sulfide ($Na_2S{\cdot}9H_2O$), sodium metasilicate ($Na_2SiO_3{\cdot}9H_2O$), sodium hydroxide (NaOH) and lithium fluoride (LiF) were applied without further purification; hydrogen fluoride (HF, 40 Wt.%), hydrochloric acid (HCl, 36.5 Wt.%) and nitric acid (HNO_3, 65 Wt.%) were adopted for pH adjusting and the acid-assisted dissolution. All the reagents were purchased from Sinopharm Chemical Reagent (Shanghai, China). Praseodymium nitrate ($Pr(NO_3)_3{\cdot}6H_2O$) was obtained from Aladdin Reagent (Shanghai, China). Deionized ultrapure water (18.25 MΩ, trace metals approximately 958 ppb) was prepared by a laboratory water purifier.

2.2 Synthesis and decomposition of pigments

2.2.1 Synthesis of zircon pigments

The pigments, Pr–$ZrSiO_4$, Fe_2O_3@$ZrSiO_4$ and CdS@$ZrSiO_4$, were synthesized by co-precipitation and high-temperature calcination. For the yellow Pr–$ZrSiO_4$, $ZrOCl_2{\cdot}8H_2O$ (32.22 g, 0.1 mol) was first dissolved in 100 mL deionized water, and then $Pr(NO_3)_3{\cdot}6H_2O$ was added with a given amount (Table 1). Another solution of $Na_2SiO_3{\cdot}9H_2O$ (34.08 g, 0.12 mol, dissolved in 200 mL water) was slowly pumped into the former solution under stirring. The mixed solution was adjusted to pH = approximately 7.0 with HCl (3.2 mol/L), and then a centrifugal water-washing was followed (Zr loss in this step, m_a). A powder was collected after the wet slurry was dried at 120°C for 16 h, and then ground and calcined at 1,050°C for 3 h after adding LiF of 5.0 Wt.% of the dry powder (the vaporized–condensed part marked as m_{v1}). A raw pigment was

Table 1 Synthesis parameters for the zircon pigments

Pr–$ZrSiO_4$	Pigments	Pr05	Pr2	Pr6	Pr12
	$Pr(NO_3)_3{\cdot}6H_2O$ (g)	0.218	0.87	2.61	5.22
	Pr/Zr (mole %)	0.5	2	6	12
	Yield (m_T, g)	18.6 ± 0.2	18.7 ± 0.3	19.1 ± 0.3	19.3 ± 0.5
Fe_2O_3@$ZrSiO_4$	Pigments	Fe10	Fe15	Fe20	Fe30
	$FeSO_4{\cdot}7H_2O$ (g)	2.78	4.17	5.56	8.34
	Fe/Zr (mole %)	10	15	20	30
	Yield (m_T, g)	19.0 ± 0.3	18.9 ± 0.4	19.8 ± 0.5	19.1 ± 0.7
CdS@$ZrSiO_4$	Pigments	Cd10	Cd15	Cd25	Cd50
	$CdSO_4{\cdot}8/3H_2O$ (g)	2.56	3.84	6.40	12.80
	$Na_2S{\cdot}9H_2O$ (g)	2.40	3.60	6.00	12.00
	Cd/Zr (mole %)	10	15	25	50
	Yield (m_T, g)	18.6 ± 0.3	19.8 ± 0.4	19.9 ± 0.6	21.6 ± 0.8

Source: Authors' own work

obtained and subsequently subjected to acid soaking in HNO_3 (10 Wt.%) to remove impurity (Zr loss in this step, m_w). Then the final pigment was collected after drying at 120°C for 2 h, and its total mass is denoted as m_T (about approximately 20 g in one synthesis).

The same procedures were conducted to prepare the red Fe_2O_3@$ZrSiO_4$ except that $FeSO_4{\cdot}7H_2O$ was used as an iron source to replace $Pr(NO_3)_3{\cdot}6H_2O$ (Table 1) and calcination was conducted at 950°C for 3 h. For the yellow CdS@$ZrSiO_4$, $CdSO_4{\cdot}8/3H_2O$ and $Na_2S{\cdot}9H_2O$ (dissolved in 150 ml water, Cd:S = 1:1) were applied for the CdS colorants. The other steps were conducted alike as for the Pr-$ZrSiO_4$ pigments. The pure zircon Pr0, Fe0 and Cd0 were synthesized without the coloring components added.

2.2.2 Decomposition of zircons and pigments

Pure zircon or zircon pigments (m_D, approximately 2.0 g) was mixed with NaOH in an agate mortar, whereas the molar ratio (R) of NaOH to zircon was set at 2, 4 and 6 to determine the minimal amount of NaOH required and at R = 18.2 for the rapid complete decomposition of the pigments. The mixture was filled into a closed corundum crucible and calcined in a muffle furnace at 700°C for 180 min at R = 2, 4, 6 and for 30 min at R = 18.2. The decomposed resultant, together with the crucible and its lid (the attached violative loss, m_{v2}), was transferred into a plastic beaker containing 200 mL deionized water, and then ultrasonic treatment was conducted for 60 min. HCl (200 mL, 5.0 mol/L) was added, and the ultrasonication continued until a clear solution was obtained. If there remained some undissolved residues, HF (2 mol/L) was added to accelerate the dissolution. The clear solution was transferred into a 500 mL volumetric flask, which was then filled up to its volumetric line with ultrapure water. If necessary, a second or third dilution was conducted to obtain a required dilution factor K_d. The final clear solution should be acidified by HCl (1.0 mol/L) rather than by pure water when K_d reached 10^2–10^4. The concentrations (C_m, C_{Zr}) of target ions were accordingly determined by ICP-OES.

2.3 Methods

Crystallographic phases of the three kinds of pigments were determined by X-ray diffraction (XRD, D8 Advance, Bruker) with a Cu $K_{\alpha 1}$ radiation source (λ = 1.540598 Å) at 40 kV and 40 mA in the scan range of 10°–70°. Morphology of the pigments was scanned using a field-emission scanning electron microscope (FE-SEM, JSM-7100F, JEOL). The contents of elements were determined by inductively coupled plasma optical emission spectrometry (ICP-OES, PlasmaQuant 9100, Analytik Jena) and mass spectrum (ICP-MS, NexION 2000, PerkinElmer). The chemical composition was performed by XPS (Escalab 250Xi). Reflectance spectra of the pigments were measured by a spectroscope (UV-2450, Shimadzu) in the wavelength range of 200–800 nm. The CIE LAB coordinates were tested by a chromometer (YS30, 3NH); L^* represents the lightness, a^* the hue from red to green and b^* the hue from blue to yellow, whereas the chroma $C* \left(= \sqrt{(a^*)^2 + (b^*)^2}\right)$ indicates the colorfulness and the hue angle h^* is calculated from $\arctan(b^*/a^*)$. The absorbance curves were transformed from the reflectance data by the Kubelka–Munk function.

3. Results and discussion

3.1 Basic properties of the zircon pigments

The crystalline composition of the red Fe_2O_3@$ZrSiO_4$ and yellow CdS@$ZrSiO_4$ as two HMZPs, and the yellow Pr–$ZrSiO_4$ as an ISZP, is demonstrated in Figure 1. The Pr–$ZrSiO_4$ pigments possess the primary phase of tetragonal $ZrSiO_4$ (ICDD # 06-0266, $I4_1$/amd) and a minor phase of ZrO_2. Because the larger Pr^{4+} cations (96 pm in radius) substitute the smaller octa-coordinated Zr^{4+} (84 pm), the strongest diffraction peaks of the (101) and (200) planes (2θ = 20.125° and 26.980°, respectively) shift to smaller angles with Pr increasing from 2% to 12% (see the magnified patterns in Figure A1), indicating the gradual expansion of the unit cell of $ZrSiO_4$. For the two HMZPs, $ZrSiO_4$ is also a dominant phase (except in Cd50) and, however, tetragonal and monoclinic ZrO_2 (t-ZrO_2 and m-ZrO_2) emerge concomitantly in a considerable amount; trace amount of SiO_2 is observed only in the Fe_2O_3 pigments. Compared with the Pr yellow pigments, an excessive introduction of Fe_2O_3 and CdS (as well as sulfur) can inhibit the crystallization of $ZrSiO_4$, although adequate chromophores are required to guarantee acceptable chroma in final pigments.

Figure 2 represents the morphology of the most chromophore-concentrated pigments, Pr12, Fe30 and Cd50. As multiple phases coexist in these pigments, $ZrSiO_4$ and ZrO_2

Figure 1 XRD patterns for (a) Pr–$ZrSiO_4$, (b) Fe_2O_3@$ZrSiO_4$ and (c) CdS@$ZrSiO_4$. The sole peak residing around 24 in the Cd10–50 cannot match any possible phase in the database

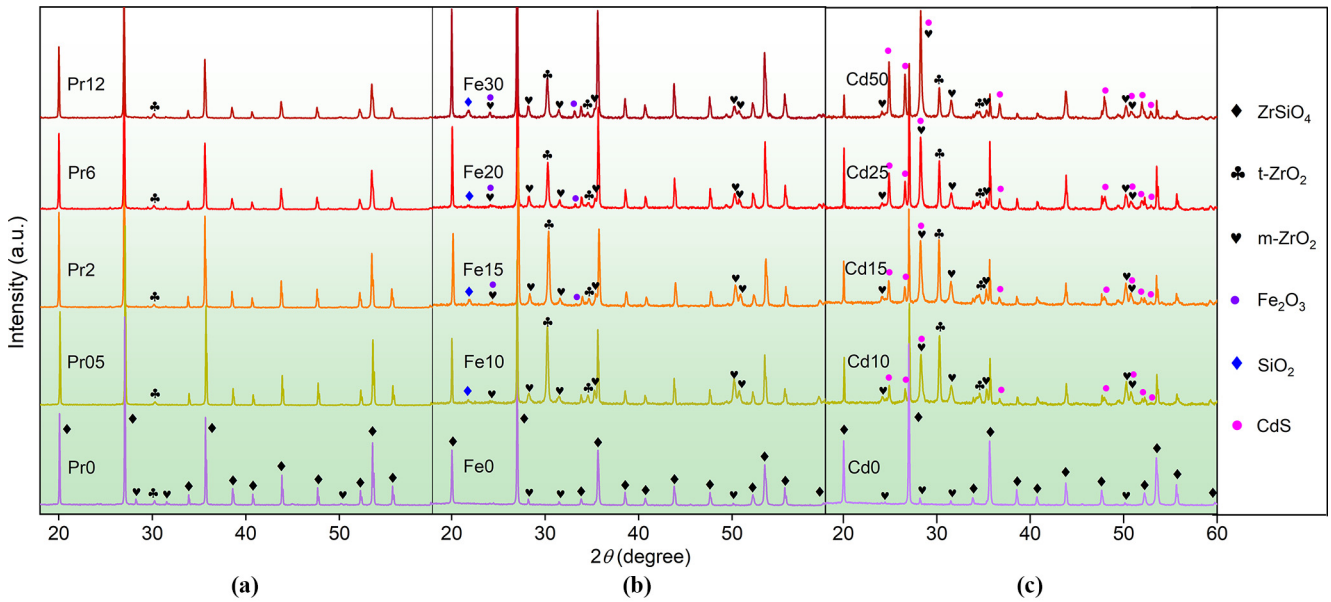

Source: Authors' own work

Figure 2 SEM micrographs of the most chromophore-concentrated pigments

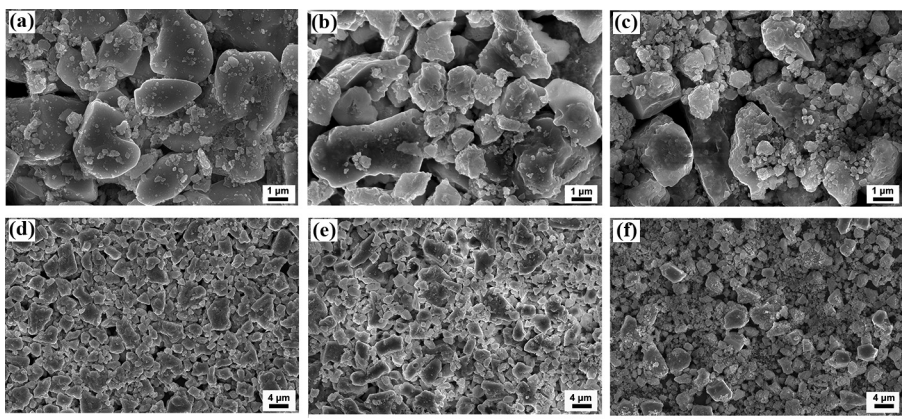

Notes: (a) and (d) Pr12; (b)–(e) Fe30 and (c)–(f) Cd50
Source: Authors' own work

(or SiO_2) cannot be well discriminated from each other by morphology in the microscopy. Empirically, the large particles are attributed to zircon crystals, which partially exhibit a typical shape of tetragonal dipyramid $ZrSiO_4$ crystals (Lei *et al.*, 2015) and have average sizes of 2–7 μm like those reported for similar zircon pigments. For the chromophores Fe_2O_3 and CdS, they have been successfully embedded into the zircon matrix (excess was removed by acid washing in synthesis) and thus cannot be directly observed in the final exposed crystals.

Light reflection–absorption of the pigments is demonstrated in Figure 3. For the Pr–$ZrSiO_4$ pigments, they render hues from primrose to brilliant yellow as Pr increases from 0.5% to 12%; the yellowness originates from the high reflectance in the yellow-to-red region of 550–700 nm and the strong absorption in the ultraviolet-to-green region around 300–500 nm. For the red Fe_2O_3@$ZrSiO_4$ pigments, the absorption onset occurs at about 550 nm, corresponding to a bandgap of 2.25 eV for hematite, whereas the significant absorption at 600–800 nm from the *d*–*d* transition of Fe^{3+} severely impair the red hue (Piccinin, 2019; Fouda *et al.*, 2012), making it deviate much from a brilliant red. The hue in the CdS@$ZrSiO_4$ pigments varies from brilliant yellow to reddish orange due to the strong reflectance at 570–800 nm and high absorption below 500 nm. Correspondingly, as the coloring centers increase, all three types of pigments equally exhibit a deepened hue, with b^* increasing from 36.93 to nearly 60 in the Pr yellow and slightly from 57.22 to 59.60 in the CdS yellow and a^* transcending over 21 from a modest 5.22 in the Fe_2O_3 red (Table 2); all the hue angles

Figure 3 Reflection and absorption spectra (a)–(d) Pr–$ZrSiO_4$, (b)–(e) Fe_2O_3@$ZrSiO_4$ and (c)–(f) CdS@$ZrSiO_4$

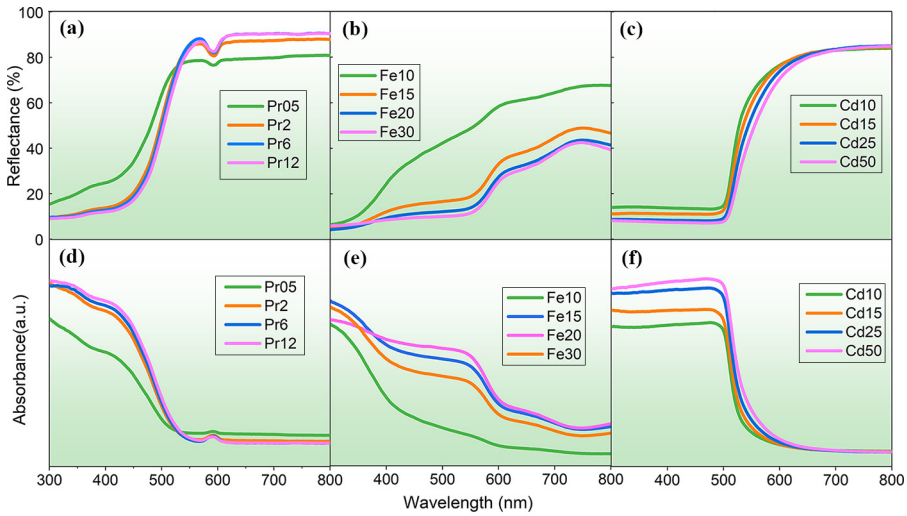

Source: Authors' own work

Table 2 Chromatic parameters of the zircon pigments (the pivotal hue parameters for a specific color are marked in italics)

Zircon pigments		L^*	a^*	b^*	C^*	h^*
Pr–$ZrSiO_4$ (ISZP)	Pr05	89.23	–6.56	*36.93*	37.51	–79.93
	Pr2	89.46	–4.46	*53.77*	53.95	–85.26
	Pr6	88.73	–2.89	*58.87*	58.94	–87.19
	Pr12	87.69	–1.00	*59.70*	59.71	–89.04
Fe_2O_3@$ZrSiO_4$ (HMZP)	Fe10	75.67	*5.22*	16.96	17.75	72.89
	Fe15	57.83	*14.48*	13.85	20.04	43.73
	Fe20	53.08	*15.54*	13.55	20.62	41.09
	Fe30	55.79	*21.34*	18.17	28.03	40.41
CdS@$ZrSiO_4$ (HMZP)	Cd10	81.12	13.23	*57.22*	58.73	76.98
	Cd15	80.53	15.67	*59.33*	61.36	75.21
	Cd25	77.55	19.21	*59.60*	62.62	72.14
	Cd50	75.08	23.26	*58.15*	62.63	68.20

h^* and chroma C^* exhibit a substantial variation, hence giving notable macroscopic improvement in hue as shown in Figure 4.

3.2 Pigment decomposition and encapsulation efficiency

To determine the encapsulation efficiency, a prerequisite is to decompose the zircon pigments into clear solutions for subsequent accurate quantitative analysis. As stated in the introduction, zircon is an extraordinarily robust matrix and some common routes become ineligible for this target. We here adopted an optimized strategy, surplus alkali-decomposition and strong acid dissolution (referred to as strong-acid dissolution [SAD2]), to treat the pigments and decomposed resultants, respectively. Because the decomposition is easily subject to the calcination temperature and alkali metal fluxing agents (FAs), tens of silicate or zirconate resultants (such as $Na_2ZrSi_2O_7$ and $Na_4Zr_2Si_3O_{12}$) have been reported (Abdelkader *et al.*, 2008; Sun *et al.*, 2019; Zhang *et al.*, 2012; Biswas *et al.*, 2010) and some cannot be well dissolved in water.

Excess NaOH as an effective FA has reduced the thermal decomposition temperature to only 700°C and also facilitates the dissolution of decomposed resultants into real solutions. The thermal decomposition is affected by the amount of NaOH, as expressed in Formula (1)–(6). When the molar ratio of FA to zircon (or pigments) R is set at 2–4, zircon is just slightly decomposed, and only trace Na_2SiO_3 and Na_2ZrO_3 are generated [Figure 5(a)]. Na_2ZrSiO_5 usually emerges as an intermediate phase and continues to react with NaOH if it is provided in adequacy. At a higher R = 6, zircon can be decomposed into Na_4SiO_4 and Na_2ZrO_3, which, together with the dissoluble Na_2SiO_3, can be well dissolved in a strong acidic solution (Table 3). The decomposition is enhanced and thus finished within only 30 min. A higher R of 18.2 (i.e. mass ratio of 4:1) is, therefore, applied to achieve sufficient decomposition while the products can be more easily dissolved.

$$(R = 2.0)\ ZrSiO_4 + 2NaOH = Na_2ZrSiO_5 + H_2O \quad (1)$$

$$Na_2ZrSiO_5 + 2NaOH = Na_2SiO_3 + Na_2ZrO_3 + H_2O \quad (2)$$

$$(R = 4.0)\ ZrSiO_4 + 4NaOH = Na_2ZrO_3 + Na_2SiO_3 + 2H_2O \quad (3)$$

$$Na_2SiO_3 + 2NaOH = Na_4SiO_4 + H_2O \quad (4)$$

$$(R = 6.0)\ ZrSiO_4 + 6NaOH = Na_2ZrO_3 + Na_4SiO_4 + 3H_2O \quad (5)$$

$$ZrSiO_4 + Na_4SiO_4 = Na_2ZrSiO_5 + Na_2SiO_3 \quad (6)$$

When the most chromophore-concentrated Pr12, Fe30 and Cd50 are decomposed, there emerge three low-crystallinity phases (Na_4SiO_4, Na_2ZrO_3 and Na_2SiO_3) in final resultants, whilst trace zircon is still observed but can be dissolved by the concomitant NaOH in the first ultrasonication treatment [Figure 5(b)]. Figure 5(c) and (d) demonstrates the pigments before and after complete dissolution by HCl. Dissolubility of

Figure 4 Photographs of the zircon pigments

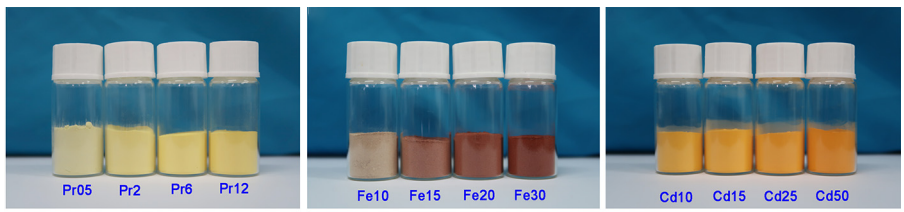

Notes: (a) Pr–$ZrSiO_4$; (b) Fe_2O_3@$ZrSiO_4$; (c) CdS@$ZrSiO_4$
Source: Authors' own work

Figure 5 (a) XRD patterns for pure zircon after decomposition at R = 2, 4 and 6; (b) the patterns for the decomposed Pr12, Fe30 and Cd50 at R= 18.2; (c)–(d) macroscopic appearance of pure zircon and the pigments before and after decomposition

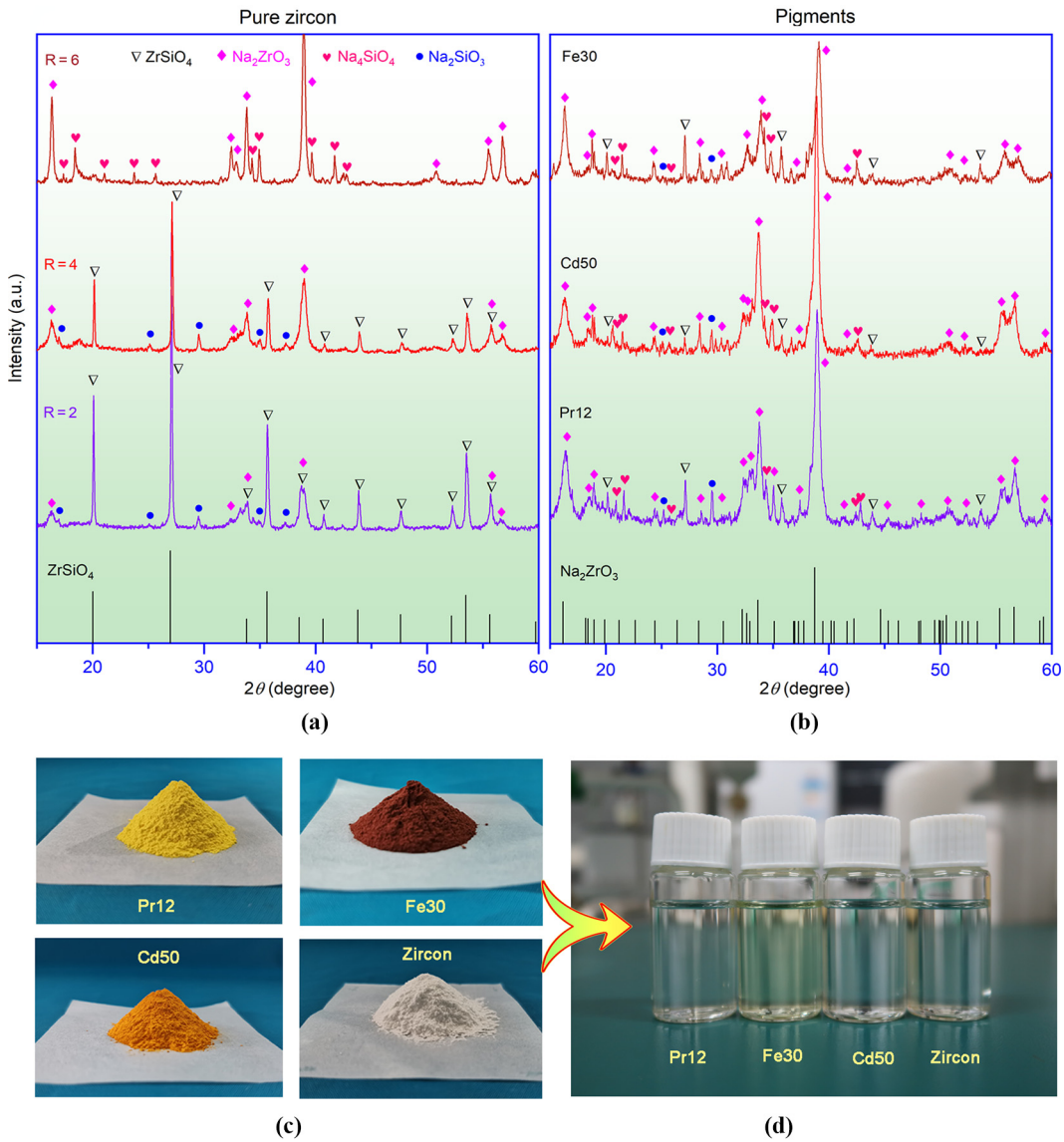

Source: Authors' own work

Table 3 Dissolubility of the alkali-decomposed products from pure zircon and the zircon pigments. Some properties were summarized by the authors and from ref. (Abdelkader *et al.*, 2008; Zhang *et al.*, 2012; Liu *et al.*, 2016)

Decom. products	Na_2SiO_3	Na_4SiO_4	Na_2ZrO_3	Na_2ZrSiO_5	$ZrOCl_2$
Water dissoluble	√	√	×	×	√
Acid dissoluble	√	√	√	√	√

Note: Indissoluble or slight dissoluble is labeled as "×" and otherwise as "√"
Source: Authors' own work

the decomposed products and the dissolution process are presented in Table 3 and by Formula (7)–(10), respectively.

$$Na_2SiO_3 + 2H_2O = H_2SiO_3 + 2NaOH \quad (7)$$

$$Na_4SiO_4 + 4HCl = H_4SiO_4 + 4NaCl \quad (8)$$

$$Na_2ZrO_3 + 4HCl = ZrOCl_2 + 2NaCl + 2H_2O \quad (9)$$

$$ZrOCl_2 + 2H_2O = ZrO(OH)_2 + 2HCl \quad (10)$$

Accordingly, two vital indices are proposed and calculated to evaluate the encapsulation efficiency of the coloring components in the zircon matrix: the relative encapsulation efficiency, α_{Re}, and the absolute encapsulation efficiency, α_{Ab}. The former, α_{Re}, is defined as the molar ratio of a central coloring component (i.e. Pr, Cd and Fe) to Zr (mainly from the zircon matrix and trace ZrO_2 is omitted). In contrast, the absolute encapsulation efficiency, α_{Ab}, is defined as the ratio of a coloring component encapsulated in the final pigments to its initial amount in the starting material, such as Cd in the final CdS@$ZrSiO_4$ pigments to that in the reagent $CdSO_4{\cdot}8/3H_2O$ at the onset of synthesis. Therefore, it is more facile to determine α_{Re} as it is a process-independent index without consideration of the whole process of synthesis, whereas α_{Ab} delineates the overall relative quantity of a coloring component that has been encapsulated into zircon when the whole synthesis process is considered.

Here the element Pr in the Pr–$ZrSiO_4$ pigments is representatively presented for the calculation protocols, whereas Fe and Cd as target elements from Fe_2O_3 and CdS in the two HMZP pigments can be similarly applied to determine the two indices. The relative encapsulation efficiency α_{Re} is expressed as follows:

$$\alpha_{Re} = \frac{\frac{C_m}{M_{w(m)}}}{\frac{C_{Zr}}{M_{w(Zr)}}} = \frac{C_m \times M_{w(Zr)}}{C_{Zr} \times M_{w(m)}} \quad (11)$$

Where C_m and C_{Zr} represent the mass concentrations (in ppm) of Pr and Zr in the diluted solutions of decomposed products, M_w(m) and M_w(Zr) denote the atomic mass of Pr and Zr, respectively. The absolute encapsulation efficiency α_{Ab} is expressed by Formula (12)–(14):

$$\alpha_{Ab} = \frac{k \times m_t / M_{w(m)}}{\sum m / M_{w(m)}} = \frac{k \times m_t}{k \times m_t + (m_w + m_a + m_{v1} + m_{v2})} \quad (12)$$

$$m_t = C_m \times V \times K_d \quad (13)$$

$$k = \frac{m_T}{m_D} \quad (14)$$

Here m_t indicates the mass of Pr encapsulated in the final pigments; m_w is the lost part in the water-washing step of the precursors, m_a is the lost portion in acid-washing of the postcalcined pigments, m_{v1} and m_{v2} the volatilized factions during the calcination and decomposition, respectively; K_d represents the total dilution factor in a single or double dilution (K_d = 10 denotes 10-fold dilution for ICP-OES tests; K_d = 10^3–10^4 for ICP-MS tests; K_d = 1 for non-diluted solutions); V is the solution volume after final dilution; m_T and m_D represent the mass of the total pigments in a single synthesis and the mass used for alkali-decomposition, respectively, and their ratio gives the factor k. The volatized fraction m_{v2} in the alkali-fusion stage should be carefully collected by acid-cleaning the crucible lid, which is vital for the HMZPs that comprise volatile chromophores (like Pr, Co and V). Figure 6 further demonstrates the whole process of synthesis and decomposition of the zircon pigments and the mass divergence of a central coloring element.

The two encapsulation indices and their correlation are thereby determined for the zircon pigments (Figure 7, with data presented in Table A1). The relative efficiencies vary consistently with the chromatic changes: as the coloring components (Pr^{4+}, Fe_2O_3 and CdS) gradually increase, the values of α_{Re} are congruently augmented to enhance the chroma in all three types of pigments (see back in Figure 4 and Table 2). Conversely, the absolute efficiencies demonstrate a descending trend in all the pigments, signifying that excess chromophore cannot be encapsulated in the zircon matrix in the thermal calcination. A high absolute efficiency (e.g. >55%) is very desirable in future for high-performance inorganic pigments and probably can be achieved by the introduction of superfine and sufficiently concentrated nano-chromophores for encapsulation (Lei *et al.*, 2015).

The two indices, α_{Re} and α_{Ab}, are confirmed interconnected with each other by another parameter, K_{RA}, which is defined as the transformation coefficient and expressed as follows:

$$K_{RA} = \frac{C_{mz} \times \alpha_{Ab}}{\alpha_{Re}} \quad 15)$$

Where C_{mz} is the nominal molar ratio of a target coloring component from the chromophores to Zr in the mixed precursors before the stage of water washing. It is observed that the two types of HMZPs give extremely stable K_{RA} values ranging 0.81–0.89 [Figure 7(c) and Table A1], although all the multiple steps throughout the process of synthesis–decomposition–dissolution can generate unavoidable mass loss. Conversely, K_{RA} in the ISZP-typed Pr–$ZrSiO_4$ varies in the range of 0.67–0.85, somewhat lower in value and larger in the fluctuation amplitude than that in the two HMZPs; this should be attributed to the fact that Pr is more violative at high temperature than Cd and Fe during the thermal treatment in synthesis and decomposition (see the m_T values in Table A1 above). Overall, the two indices α_{Re} and α_{Ab} exhibit a considerably fine correlation with each other, and, more importantly, the former can be independently applied and is more facile in the value determination without consideration of the whole process of synthesis–decomposition.

Extra precautions should be taken when some analogous quantification techniques are adopted for encapsulation

Figure 6 Chart of the mass divergence of a chromophoric element throughout the process from synthesis to decomposition and to the dissolution of the zircon pigments

Source: Authors' own work

Figure 7 (a) and (b) The encapsulation efficiencies α_{Re} and α_{Ab} and (c) K_{RA}. Quantification was obtained by ICP-OES

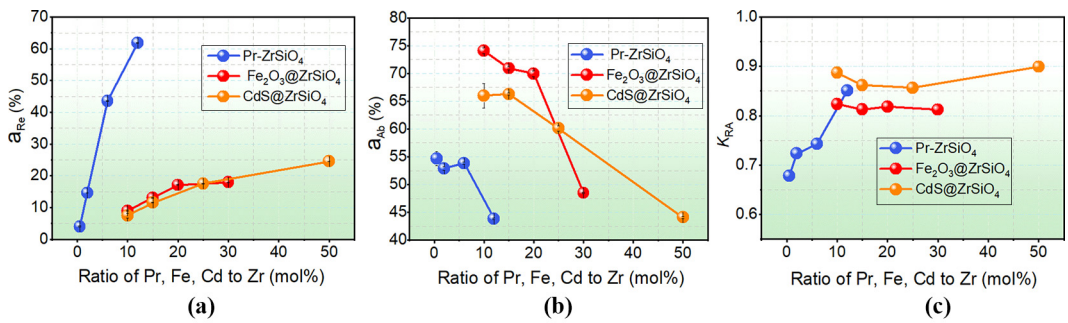

Source: Authors' own work

efficiencies. ICP-MS, in lieu of ICP-OES, is not recommendable because this quantification requires a high $K_d > 10^3$, which causes severe interference by the Si source from the ultrapure water for additional acidification (see the detailed discussion in Tables A1–A3). Additionally, XPS can bring severely underestimated data, such as α_{Re} = 0.1%–0.6% and α_{Ab} = 1%–14% (Figure A2), due to its extremely shallow detection depth below 10 nm in contrast with the much larger sizes of 2–7 μm in the zircon pigments.

In prospect, the absolute/relative encapsulation efficiencies we proposed have the potential to advance the further development of zircon pigments, which are currently mainly restricted in chroma by the suboptimal coloring centers in amount (Lei *et al.*, 2015) and can be significantly enhanced if more chromophores are encapsulated in the zircon matrix. Furthermore, the SAD2 strategy can be extended to many other robust materials akin to zircon, like the pigments Bi-doped $Ce_{1-x}Zr_xO_2$, and the phosphors of $Y_2Ce_2O_7$:Eu^{3+} and $Y_3Al_5O_{12}$:Ce^{3+} (Furukawa *et al.*, 2008; Raj *et al.*, 2014; Li *et al.*, 2021), which are also probably inhomogeneous in the microscopic scale and unsuitable for undisruptive quantitative analysis.

4. Conclusions

- The robust zircon pigments (Pr–$ZrSiO_4$, Fe_2O_3@$ZrSiO_4$ and CdS@$ZrSiO_4$) can be completely decomposed into some dissoluble resultants, mainly Na_4SiO_4, Na_2ZrO_3 and Na_2SiO_3, by the route SAD2. The ratios of the FA to pigment should exceed R = 6 for thorough thermal decomposition, which is necessitated for subsequent accurate compositional analysis via the optimal quantification technique of ICP-OES.
- The relative and absolute encapsulation efficiencies, α_{Re} and α_{Ab}, are thereby determined. The two indices can well evaluate the loss of chromophores in synthesis and the chromatic properties of final pigments. As the chromophore increases in the precursors, α_{Ab} declines drastically, and α_{Re} increases significantly in the final pigments, enhancing the pigments with a substantially improved chromaticity.
- The index α_{Re} interacts closely with α_{Ab} via the transformation coefficient K_{RA}, which maintains stably at 0.8–0.9 in the two HMZPs (Fe_2O_3@$ZrSiO_4$ and CdS@$ZrSiO_4$) and is slightly reduced to 0.67–0.85 in the ISZP-typed Pr–$ZrSiO_4$. The relative efficiency α_{Re} is a process-irrelevant indicator and, thus, more suitable for independent characterization to the heterogeneous zircon pigments.

Discussion below for the encapsulation efficiencies obtained by ICP-MS

Precautions should be taken in testing the decomposed solutions. First, the ICP-OES is strongly preferred in lieu of the ICP-MS. When the latter is applied for quantification, a much lower concentration (with $K_d > 10^3$) is required; multiple dilutions not only add many conductions (like solution acidization) but also severely enhance the undesired silicon interference from the ultrapure water (Si concentration at 20–50 ppb, in the same order of magnitude with the diluted pigment solutions required). When the dilution factor K_d exceeds 10^2, additional acidification becomes necessitated to suppress the Zr polymerization, whereas the concentrations of target elements obtained by ICP-MS often greatly deviate from the real values (Tables A2 and A3).

References

Abdelkader, A.M., Daher, A. and El-Kashef, E. (2008), "Novel decomposition method for zircon", *Journal of Alloys and Compounds*, Vol. 460 Nos 1/2, pp. 577-580.

Biswas, R., Habib, M., Karmakar, A. and Islam, M. (2010), "A novel method for processing of Bangladeshi zircon: part I: baking, and fusion with NaOH", *Hydrometallurgy*, Vol. 103 Nos 1/4, pp. 124-129.

Cannio, M. and Bondioli, F. (2012), "Mechanical activation of raw materials in the synthesis of Fe_2O_3-$ZrSiO_4$ inclusion pigment", *Journal of the European Ceramic Society*, Vol. 32 No. 3, pp. 643-647.

Chen, S., Cheng, M., Lang, Y., Wei, H. and Wang, C.-A. (2018), "Synthesis and chromatic properties of zircon encapsulated ceramic black pigment with carbon sphere as carbon source", *Journal of the European Ceramic Society*, Vol. 38 No. 4, pp. 2218-2227.

Chen, S., Fu, S., Lang, Y., Tian, C., Wei, H. and Wang, C. (2019), "Submicronic spherical inclusion black pigment by double-shell reaction sintering", *Journal of the American Ceramic Society*, Vol. 103 No. 3, pp. 1520-1526.

Fouda, M., El-Kholy, M., Moustafa, S., Hussien, A., Wahba, M. and El-Shahat, M. (2012), "Synthesis and characterization of nanosized Fe_2O_3 pigments", *International Journal of Inorganic Chemistry*, Vol. 2012, pp. 1-9.

Furukawa, S., Masui, T. and Imanaka, N. (2008), "New environment-friendly yellow pigments based on CeO_2–ZrO_2 solid solutions", *Journal of Alloys and Compounds*, Vol. 451 Nos 1/2, pp. 640-643.

Guo, D., Xie, M., Ma, N., Yang, Q., Luo, Z., Chu, Y., Zhang, Y. and Rao, P. (2018), "Synthesis and characterization of (Pr, Ce)-$ZrSiO_4$ ceramic pigments: the properties of the pigments and the effect of Ce", *Journal of the American Ceramic Society*, Vol. 102 No. 1, pp. 2619-2628.

Heydari, H., Naghizadeh, R., Samimbanihashemi, H.R. and Hosseini-Zori, M. (2013), "Synthesis and characterisation of hematite-zircon nanocomposite by sol-gel method", *Advanced Materials Research*, Vol. 829 No. 1, pp. 544-548.

Hou, Z., Xiao, Y., Shen, J. and Yu, C. (2020), "In situ rutile U-Pb dating based on zircon calibration using LA-ICP-MS, geological applications in the Dabie Orogen, China", *Journal of Asian Earth Sciences*, Vol. 192, p. 104261.

Jansen, M. and Letschert, H. (2000), "Inorganic yellow-red pigments without toxic metals", *Nature*, Vol. 404 No. 6781, pp. 980-982.

Lei, B., Qin, W., Kang, G., Peng, C. and Wu, J. (2015), "Modeling and evaluation for encapsulation efficiency of zircon-based heteromorphic encapsulation pigments", *Dyes and Pigments*, Vol. 112 No. 1, pp. 245-254.

Li, J., Ma, Z., Wang, F. and Wang, Z. (2021), "Synthesis and mechanoluminescent properties of submicro-sized $Y_3Al_5O_{12}$: ce^{3+} particles", *Chemical Physics Letters*, Vol. 775, p. 138664.

Li, P., Yang, Q. and Zhang, S. (2019), "Low temperature synthesis and performance investigation of co-doped (Cr, Co)-$ZrSiO_4$ ceramic pigments", *IOP Conference Series: Materials Science and Engineering*. Vol. 677, p. 22086.

Liu, J., Song, J., Qi, T., Zhang, C. and Qu, J. (2016), "Controlling the formation of Na_2ZrSiO_5 in alkali fusion process for zirconium oxychloride production", *Advanced Powder Technology*, Vol. 27 No. 1, pp. 1-8.

Piccinin, S. (2019), "The band structure and optical absorption of hematite (α-Fe_2O_3): a first-principles GW-BSE study", *Physical Chemistry Chemical Physics*, Vol. 21 No. 6, pp. 2957-2967.

Qin, W., Wang, K. and Zhang, Y. (2021), "Preparation of submicron CdS_xSe_{1-x}@$ZrSiO_4$ inclusion pigment and its application in ink-jet printing", *Journal of the European Ceramic Society*, Vol. 41 No. 15, pp. 7878-7885.

Raj, A.K., Rao, P.P., Sreena, T., Sameera, S., James, V. and Renju, U. (2014), "Remarkable changes in the photoluminescent properties of $Y_2Ce_2O_7$: eu^{3+} red phosphors through modification of the cerium oxidation states and oxygen vacancy ordering", *Physical Chemistry Chemical Physics*, Vol. 16 No. 43, pp. 23699-23710.

Sun, H., Song, J., Sun, S., Qu, J., Wei, L. and Tao, Q. (2019), "Decomposition kinetics of zircon sand in NaOH Sub-molten salt solution", *Transactions of Nonferrous Metals Society of China*, Vol. 29 No. 9, pp. 1948-1955.

Tang, H., Hu, Q., Jiang, F., Jiang, W., Liu, J., Chen, T., Feng, G., Wang, T. and Luo, W. (2019), "Size control of C@$ZrSiO_4$ pigments via soft mechano-chemistry assisted non-aqueous sol-gel method and their application in ceramic glaze", *Ceramics International*, Vol. 45 No. 8, pp. 10756-10764.

Tang, H., Hu, Q., Jiang, W., Liu, J., Feng, G., Chen, T., Tan, G., Zhang, X. and Miao, L. (2018), "Facile non-aqueous synthesis of high color rendering C@$ZrSiO_4$ encapsulation pigment with carbon-containing precursors as in-situ carbon sources", *Ceramics International*, Vol. 44 No. 14, pp. 16498-16506.

Ver Hoeve, T., Scoates, J., Wall, C., Weis, D. and Amini, M. (2018), "Evaluating downhole fractionation corrections in LA-ICP-MS U-Pb zircon geochronology", *Chemical Geology*, Vol. 483, pp. 201-217.

Wang, Y., Lai, F., Wang, Q., Long, Q., Wang, C., Zhang, W. and Chang, Q. (2022a), "Synthesis and chromatic properties of high color performance Pr_x-$ZrSiO_4$ (x = 0–0.1) yellow pigment", *Journal of Alloys and Compounds*, Vol. 891, p. 161932.

Wang, T., Liu, J., Jiang, W., Jiang, F., Feng, G., Miao, L., Zhang, Q., Wu, Q. and Lao, X. (2022b), "Fluorine-free synthesis and characterization of vanadium-zircon (V–$ZrSiO_4$) turquoise ceramic pigment by a low temperature solid state reaction route", *Ceramics International*, Vol. 48 No. 16, pp. 24044-24055.

Wang, S., Peng, C., Xiao, H. and Wu, J. (2015), "Microstructural evolution and crystallization mechanism of zircon from frit glaze", *Journal of the European Ceramic Society*, Vol. 35 No. 9, pp. 2671-2678.

Wang, C., Wang, Q., Liu, K., Liu, J., Wang, Y., Yang, Y. and Chang, Q. (2020), "Synthesis, characterization and application of submicron $ZrSiO_4$ powder via sol-gel-microemulsion-hydrothermal method", *Journal of Alloys and Compounds*, Vol. 828, p. 154332.

Yang, Q., Li, P. and Zhang, S. (2021), "Low temperature synthesis of green submicro Cr-$ZrSiO_4$ ceramic pigments by solid-state method", *International Journal of Applied Ceramic Technology*, Vol. 18 No. 2, pp. 345-352.

Zhang, A., Mu, B., Wang, X. and Wang, A. (2019), "Microwave hydrothermal assisted preparation of $CoAl_2O_4$/kaolin hybrid pigments for reinforcement coloring and mechanical property of acrylonitrile butadiene styrene", *Applied Clay Science*, Vol. 175, pp. 67-75.

Zhang, W., Wang, Q., Chen, X., Li, X., Long, Q., Wang, C., Liu, K., Wang, Y. and Chang, Q. (2021), "Synthesis of high color performance V-$ZrSiO_4$ blue pigment with low doping amount via inorganic sol–gel route", *Advanced Powder Technology*, Vol. 32 No. 9, pp. 3355-3363.

Zhang, J., Wang, L. and Jiang, D. (2012), "Decomposition process of zircon sand concentrate with CaO-NaOH", *Rare Metals*, Vol. 31 No. 4, pp. 410-414.

Appendix

Figure A1 XRD patterns for the Pr–$ZrSiO_4$ pigments around the planes of (101) and (200), respectively

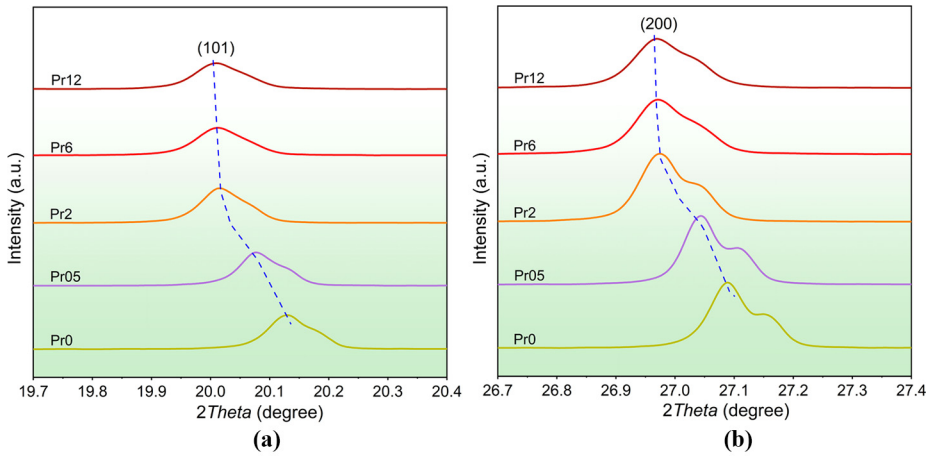

Source: Authors' own work

Figure A2 (a) and (b) The relative and absolute efficiencies α_{Re} and α_{Ab} and (c) the Zr/Si ratios as a function of C_{ms}. The contents of the elements were determined by XPS

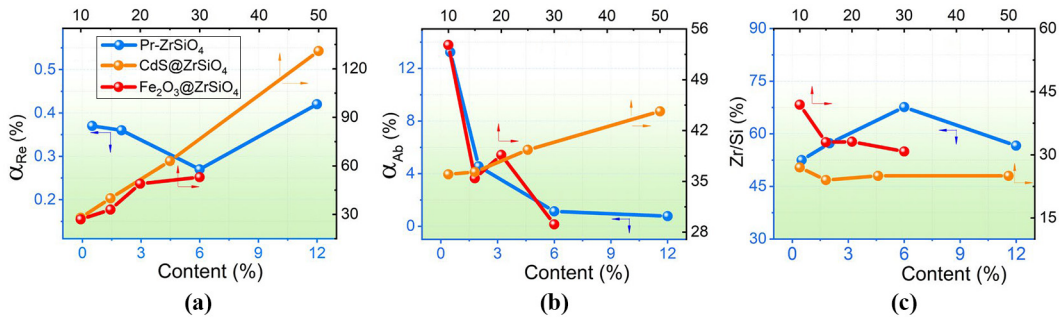

Source: Authors' own work

Table A1 The α_{re}, α_{Ab} and Zr/Si ratios in the three series of pigments tested by ICP-OES

Pigments	C_{ms} (%)	Zr/Si (%)	α_{Re} (%)	α_{Ab} (%)	K_{RA} (%)	Average K_{RA} (%)
Pr05	0.5	78.82 ± 1.28	0.40 ± 0.12	54.65 ± 1.30	67.80	74.86
Pr2	2	81.39 ± 0.52	1.46 ± 0.02	52.88 ± 0.33	72.34	
Pr6	6	81.78 ± 0.46	4.35 ± 0.14	53.86 ± 0.22	74.24	
Pr12	12	84.09 ± 0.09	6.18 ± 0.01	43.83 ± 0.14	85.05	
Fe10	10	81.91 ± 0.51	8.99 ± 0.12	74.05 ± 0.50	82.37	81.67
Fe15	15	75.03 ± 0.46	13.09 ± 0.09	70.92 ± 0.32	81.27	
Fe20	20	78.12 ± 0.58	17.09 ± 0.09	69.93 ± 0.51	81.84	
Fe30	30	80.29 ± 0.98	17.91 ± 0.01	48.49 ± 0.09	81.22	
Cd10	10	83.99 ± 0.10	7.44 ± 0.74	65.98 ± 2.24	88.68	87.60
Cd15	15	85.44 ± 0.44	11.54 ± 0.04	66.29 ± 0.18	86.17	
Cd25	25	87.48 ± 0.03	17.54 ± 0.10	60.09 ± 0.44	85.65	
Cd50	50	83.53 ± 0.64	24.52 ± 0.04	44.09 ± 0.18	89.91	

Note: It is explicit that the Zr/Si ratios tested via ICP-OES in all three types of pigments vary within 75%–87% (fluctuation only at approximately 16%), much smaller than those in the XPS-based data (45%–68%, fluctuation as high as approximately 51%, see Figure A2)
Source: Authors' own work

Table A2 The composition of the ultrapure water used in this work

Metals	Ca	K	Na	Si	Fe	Mg	Ni	Cr	Al	Total
Content (ppb)	462.09	239.51	92.17	*34.25*	26.35	2.28	0.58	0.39	0.30	957.82
Error (ppb)	10.76	16.07	1.84	*0.02*	0.44	0.02	0.08	0.01	0.01	–

Note: The water was produced by a laboratory water purifier and well satisfies standard requirements (Resistance 18.25 MΩ). Data were tested by ICP-MS
Source: Authors' own work

Table A3 Comparison of ICP-OES and ICP-MS for quantitative analyses of pure zircon

Solution for testing	ICP type	Dilution Factor, K_d	Unit	Theoretical conc. Zr	Theoretical conc. Si	Tested conc. Zr	Tested conc. Si
Commercial	*ICP-OES*	*×10*	*ppm*	*199.06*	*61.10*	*179.07 ± 0.70*	*50.24 ± 0.16*
Zircon (decomposed)	ICP-MS	×1,000	ppb	1990.6	611.00	1,440.36 ± 76.02	536.31 ± 14.67
	ICP-MS	×10,000	ppb	199.06	*61.10*	*30.03 ± 0.60*	*77.16 ± 1.57*
Zr-Si mixed solution	*ICP-OES*	*×10*	*ppm*	*91.30*	*28.10*	*88.78 ± 1.05*	*23.92 ± 0.13*
	ICP-MS	×1,000	ppb	913.00	281.00	750.46 ± 19.43	360.67 ± 20.50
	ICP-MS	×10,000	ppb	91.30	*28.10*	*18.38 ± 0.61*	*64.63 ± 0.69*

Notes: The data labeled in blue for the silicon contents indicate that ultrahigh dilution will make the silicon content descend to the same order of magnitude with that in the ultrapure water, as shown in Table A2). The zircon was recognized as a pure $ZrSiO_4$ sample and a mass of 2.00 g was applied for decomposition and prepared into a solution of 500 mL, with a subsequent dilution of K_d-folds; the Zr–Si mixed solution was prepared with $ZrOCl_2{\cdot}8H_2O$ (5.00 mmol, 1.611 g) and $Na_2SiO_3{\cdot}9H_2O$ (5.00 mmol, 1.420 g) dissolved in 500 mL water
Source: Authors' own work

Corresponding author
Binglong Lei can be contacted at: lei@hubu.edu.cn